JOURNAL OF MATERIALS SCIENCE **40** (2005) 3517–3522

Geometrical features of wear debris

Part I *Erosion of ductile steel by solid particle impingement*

A. W. MOMBER*
RWTH Aachen, BGMR, Faculty of Georesources and Materials Technology, Brunsstraße 10, D-21073 Hamburg, Germany
E-mail: andreas.momber@t-online.de

Y. C. WONG
School of Engineering and Science, Swinburne University of Technology, P.O. Box 218, Melbourne, Victoria 3122, Australia

Image analysis software was used to analyse the geometry of debris formed during the erosion of low-carbon steel by impinging solid particles. Depending on the two-dimensional aspect ratio (ratio between debris height and debris width), three different debris types could be distinguished. The most frequent type observed was a platelet-type debris as suggested by the Bellman-Levy (1981) model. This wear debris shape type covered about 60% of all acquired debris. Plain micro-machining according to Finnie's (1959) suggestion played a negligible role only, but other processes, namely ploughing as suggested by Winter and Hutchings (1974), were more important. The statistically estimated mean debris size was about 14 μm. About 92% of all wear debris had sizes smaller than the target material grain size. This result supports the figure that 'secondary' removal modes—lip or platelet, respectively, detachment from crater rims—were responsible for material removal.

1. Introduction

Erosion of metals by solid particles is a notable economic problem. It is not only the unwanted wear of structures due to particle erosion [1], but also the useful application of this erosion mode for machining processes [2], that makes it important to understand the fundamental material removal modes involved in this erosion type. Shewmon and Sundararajan [3] subdivided modes for the erosion of metals into five types, namely cutting, fatigue, shear localization, adiabatic shear-induced spalling, and delamination. The classical cutting model is the 'micro-cutting' model introduced by Finnie [4] who assumed that metal removal by erosion involves cutting similar to that found in machining, in which a negative, or zero, rake angle exists. This mode would finally form chip-like debris with a high length-to-width (aspect) ratio. It was, however, shown by Winter and Hutchings [5] due to controlled impact experiments with sharp steel projectiles that such a plain cutting mechanism occurred only rarely. This conclusion was also drawn by Kosel *et al*. [6] from erosion tests on stainless steel who found that most of the debris did not exhibit a characteristic lamellae shape as would be expected for micro-machining. These authors suggested that the high roughness of the eroded surface (even on a scale similar to the size of the debris) avoided a plain micro-cutting process. Another explanation was delivered by Winter and Hutchings [5] who found that a 'ploughing' mechanism that caused the extrusion of a lip at the exit side of crater was a dominant removal mode in soft metals. A critical threshold erodent velocity was required in order to introduce ploughing. Bellmann and Levy [7] introduced a so-called 'platelet' model. In this phenomenological model, a combined forging-extrusion mechanism which produced highly-distressed platelets of target material that were knocked off from the surface by succeeding impacts was assumed to be responsible for the erosion. This model held also for high impact angles. Both mechanism mentioned above - ploughing and platelet formation—require the successive impact of multiple erodent particles, basically in order to detach the debris (lips and platelets, respectively) from the surface. A combination of plate-like debris formation and micro-machining was reported in [6] for the erosion of stainless steel by aluminium oxide, whereby the plate-like debris were predominantly formed at higher angles of incidence. Hammarsten *et al*. [8] performed a detailed study into the morphology of wear fragments. They recovered erosion debris directly from the surface by a tape method. Therefore, only the rear side of the debris could be evaluated. With respect to morphology, these authors subdivided debris analysed with scanning electron microscopy into three groups, namely chips,

*Author to whom all correspondence should be addressed.

flakes, and tufts. The authors did not measure the aspect ratio, but only the average diameter of the debris. However, from the original photographs published in [8] it can be concluded that 'chips' had a rather high aspect ratio (between 3 and 4), and 'flakes' had a moderate aspect ratio (ca. 1.5). The geometry of 'tufts' was rather irregular, and a reliable aspect ratio could not be estimated from the corresponding photographs. The concentration of chips (flow-type) in the debris sample was found to be 15% for shallow impact, and 30% for normal incidence [8]. The concentration of 'flakes' was independent of the impact angle, it was always about 44%. Tscherny *et al*. [9] obtained contrary results. They noted the formation of platelets with a maximum cross section of 1 mm^2 and thickness values between 2 and 5 μm. This shape did not change if erosion conditions changed. From distribution charts for length and width of the debris published in the original paper, an average aspect ratio of about 2.4 can be calculated. Momber *et al*. [10] applied the parameters of debris formed during the hydro-abrasive erosion of cast iron for efficiency calculations.

2. Experimental set-up

All tests were performed with hot-rolled low-carbon steel. The steel contained the following alloying elements (given in mass%): carbon (0.1), phosphorus (0.03), manganese (0.50), silicon (0.03), sulphur (0.03), aluminium (0.10), titanium (0.04), micro alloys (0.01). The average grain size, estimated with a metallurgy microscope, was 25 μm. The grain structure is shown in Fig. 1. The mechanical properties of the material are listed in Table I. The specimens were cut off from a standard plate by sawing; their dimensions were 150 mm × 40 mm × 3 mm. All specimens were stored in a desiccator in order to prevent atmospheric corrosion.

The grit blasting experiments were performed in a commercial blasting cabinet using an air pressure of 0.475 MPa and a nozzle diameter of 8 mm. The particle velocity was not estimated. Aluminium oxide with a mean particle size of $d_{50} = 165$ μm was used as erodent. The particle size distribution is listed in Table II, whereas the particle shape is shown in Fig. 2. The chemical composition of the erodent material is listed in Table III. The erodent feed rate was 19.3 g/s, and the flux rate was 1.54 g/(s·cm^2). Each specimen was blasted at an exposure time of 60 s, at an angle of 90°, and with a stand-off distance between nozzle exit and specimen surface of 10 mm. The specimen weight was measured before and after each erosion test, and the weight loss, ΔW, was estimated. The mass balance used was a 'Sartorius Analytic' with a maximum weight capacity of 200 g and a precision of ±200 μg. The specific mass removal, ΔM, was also estimated as follows:

$$\Delta M = \frac{\Delta W}{A_S} \tag{1}$$

In the equation, A_S is the eroded cross section. All estimated values are listed in Table IV.

The mixture of steel wear debris and fractured erodents was collected during the grit blasting performance

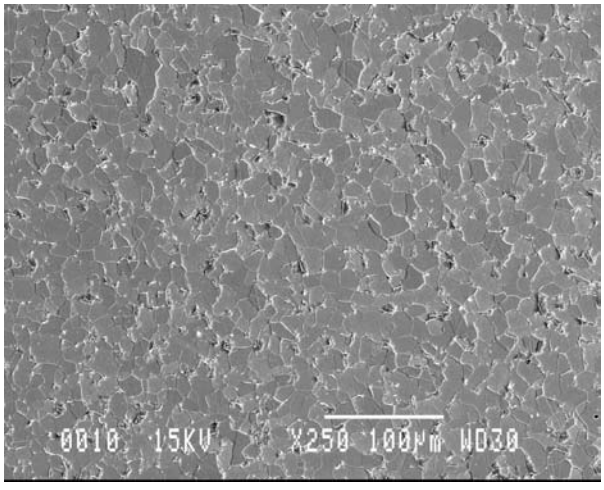

Figure 1 Grain structure of the specimen material (metallurgical microscope image), scale bar: 100 μm

TABLE I Specimen properties

Property	Value
Density	7860 kg/m^3
Elongation	33%
Grain structure[a]	ASTM 8/100
Vickers hardness	126 kg/mm^2
Tensile strength	350 MPa
Yield strength	260 MPa

[a]Reichert metallurgical microscope type MeF.

TABLE II Erodent particle size distribution

Sieve range (μm)	Absolute retained (%)
<75	4.6
75–150	13.9
151–300	65.5
>300	16.0
Total	100

TABLE III Chemical composition of the abrasive material

Element	Percentage
Al_2O_3	96.4
TiO_2	2.5
SiO_2	0.7
Fe_2O_3	0.1
MgO	0.2
CaO	0.05
Na_2O	0.01
Fe (soluble)	0.1

TABLE IV Process parameters and erosion results

Parameter	Value
Operating pressure (MPa)	0.475
Exposure time (s)	60
Stand-off distance (mm)	10
Weight loss (mg)	761
Specific weight loss (mg/mm^2)	0.12

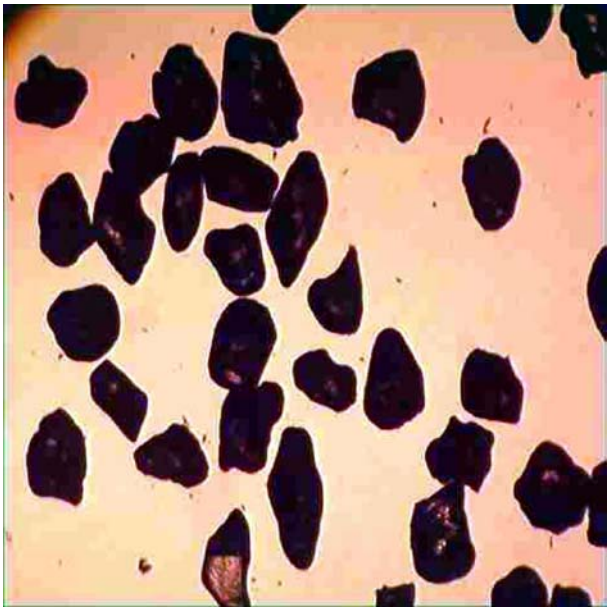

Figure 2 Erodent particles used for the experiments, image width: 1.8 mm.

in a specially designed plastic chamber. The steel specimen debris were separated from the aluminium oxide fragments using a demagnetiser; they were then dried and ultrasonically cleaned. Three random samples from the collected debris quantity were separated and analysed. A total number of 806 debris was analysed. The weight of the debris sample was estimated independently of the weight loss estimation of the specimen. The samples were spread evenly on a clean thin glass plate which was placed under the microscope. Suitable magnification and illumination conditions were adjusted in order to obtain an optimum view. A representative area of the particles under the microscope was selected before the image was finally captured. This procedure was repeated for other representative areas and for all samples. Systematic EDX-measurements were performed in order to check erodent fragments adhering to separated wear debris. However, contamination through erodent material happened to less than 2% of all wear debris. An image analyser equipped with an optical microscope 'CH-32-Olympus' and a digital camera 'PML-76' which was connected to a standard PC was used for the image analysis of individual debris. In detail, the system measured height (HD) and width (WD) of the captured objects, whereby HD was the projection in Y-direction, and WD was the projection in X-direction by definition. The cross sectional area (A) of the captured objects (given in μm^2) was independently calculated. The two dimensional geometry (aspect ratio) of the debris was defined as follows:

$$\Phi = \mathrm{HD}/\mathrm{WD}. \tag{2}$$

This parameter is dimensionless. Particles with ratios $1.0 < \Phi < 1.5$ were denoted 'platelets', whereas particles with ratios $\Phi > 4$ were denoted 'chips'. The average size of the debris was defined as follows:

$$S = \frac{\mathrm{HD} + \mathrm{WD}}{2}. \tag{3}$$

TABLE V Statistics of debris geometry parameters

Shape parameter	Statistical parameter				
	Mean value	Standard deviation	Variance	Maximum value	50%-value[a]
Height (HD) (μm)	15.5	11.4	130.3	127	—
Width (WD) (μm)	14.7	9.7	94.8	78	—
Area (A) (μm^2)	160.7	407.5	166,020	8,000	55
Aspect ratio (Φ) (–)	1.10	0.55	0.30	4.6	1.25
Average size (S) (μm)	14.1	10.1	101.4	97	9.9

[a]graphically estimated.

This parameter is given in μm. A commercial software 'Freelancer' was adapted to convert and calculate all image parameters. The following statistics parameters were estimated for the debris shape parameters: mean value, standard deviation, variance, and 50%-distribution value. These results are listed in Table V.

Additional scanning electron microscope images were taken from selected samples in order to further evaluate the debris morphology.

3. Results and discussion

Fig. 3 shows two examples of captured objects. Fig. 3a illustrates the original mixture of collected samples that is composed of wear debris and erodent fragments. A notable difference in size could be noted. The wear debris were one order of magnitude smaller than the erodents. This agreed with results in [9] where a ratio between erodent diameter and debris diameter of 30:1 was found. Fig. 3b illustrates the situation after the wear debris were separated from the erodent fragments. According to the aspect ratio (Φ), Three types of debris geometry could be distinguished:

- type (i): debris with low Φ-values ($1 < \Phi < 1.5$);
- type (ii): debris with moderate Φ-values;
- type (iii): debris with high Φ-values ($\Phi > 4$).

The case (i) corresponded to platelet-type-debris according to the Bellman-Levy model [7], whereas the case (iii) corresponded to chip-type-debris as typically formed during micro-machining processes. The case (ii), however, may be related here to a ploughing mechanism as a first approximation. The quantitative rating of the individual erosion modes was made based on the aspect ratio. The results are illustrated in Fig. 4. Figure 4a shows a debris histogram where the percentage of debris in plotted against the aspect ratio. It can be seen that about 60% of all debris belong to the debris type (i). Fig. 4b shows the cumulative debris distribution. Also shown in this graph are the statistical mean aspect ratio and the (graphically estimated) 50%-value. The statistical mean aspect ratio is $\Phi = 1.1$, and the 50%-ratio is $\Phi_{50} = 1.25$; both values correspond to the definition for platelet-shaped debris. Micro-machining chips, however, are formed with a very low frequency. Their amount is negligibly small (about 1.1%). If, however, the group $\Phi = 2$–4 would be included into to the 'chip' definition, the results (15.6%) would agree with

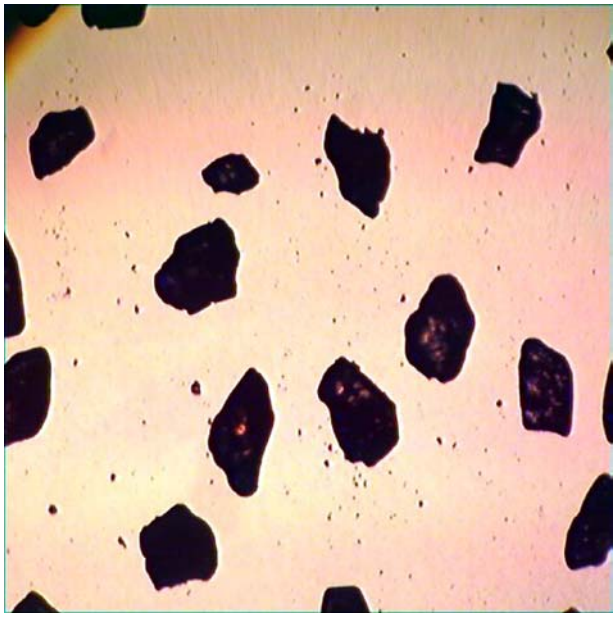

(a)

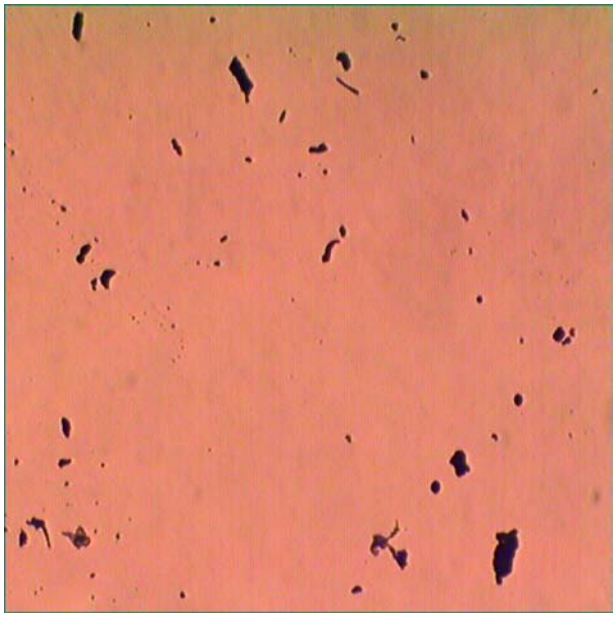

(b)

Figure 3 Images of captured objects: (a) Mixture of wear debris and erodent fragments, image width: 1.8 mm and (b) Sample of separated wear debris as used for analysis, image width: 1.1 mm

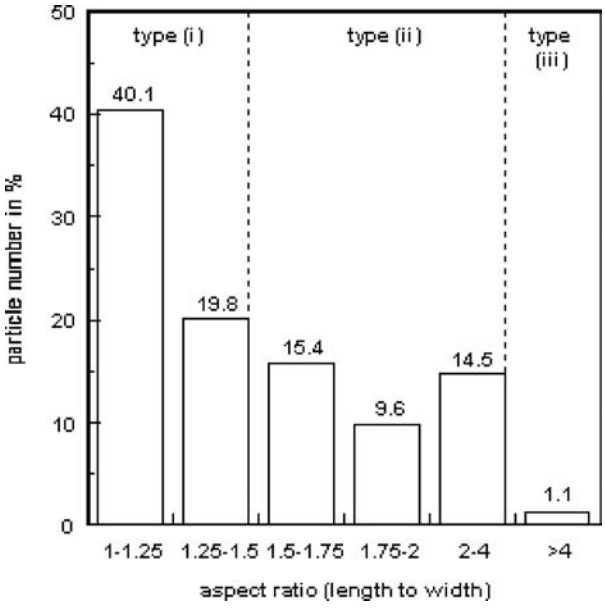

(a)

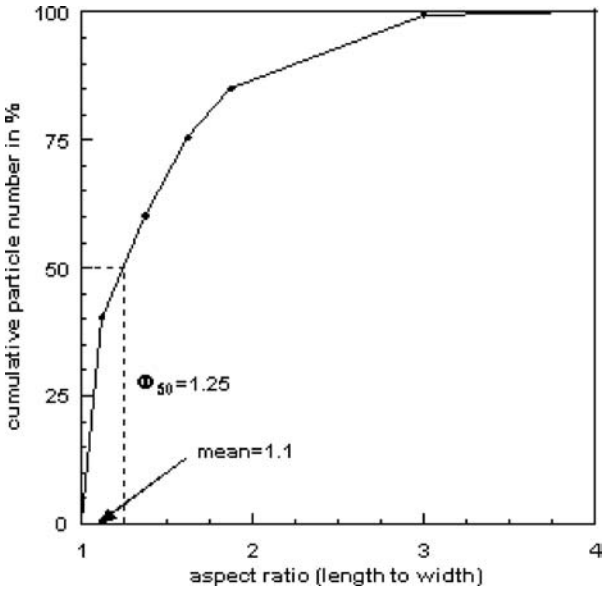

(b)

Figure 4 Aspect ratio distribution of the analysed wear debris: (a) Histogram and (b) Cumulative distribution.

those in [8] where a chip concentration between 15 and 22% was found for perpendicular impact.

Scanning electron microscope images taken from the erosion sites delivered further information about the debris morphology. Fig. 5 shows two typical scanning electron microscope images of eroded surfaces. At high magnification, as shown in Fig. 5a, individual tracks with broken edges could be observed suggesting that material was partly removed by lip extrusion, or detachment, respectively. This process is considered to be ploughing. The average track width was about 10 μm which was one order of magnitude smaller than the mean erodent diameter. The wear track were not directed to a certain direction, but ran rather irregular; this can be seen in Fig. 5a. Another situation is illustrated in Fig. 5b showing an accumulation of small plates with dimensions of about 15 μm. The platelets seem to be still attached to the surface, but are already separated by microcracks. Similar photographs can be found in [7]. Evidence for plain micro-cutting is given in Fig. 6a showing the lamella structure of a flow-type chip; this is a typical wear debris of type (iii) produced during a micro-machining process. Such clearly defined lamellae were found in [6] on debris surfaces formed during abrasion and scratching tests. Fig. 6a also shows wear debris of type (i): several small, platelet-shape debris can be seen. More of these platelets, with a typical size of 10 μm, are shown in Fig. 6b. This size corresponds to the dimensions of the attached plates shown in Fig. 5b. In the lower section of Fig. 6b, a long debris is visible which is actually a composition of adhering platelets. (This case occurred very rarely only and would be misinterpreted as a debris type (iii) by the image analysing software.) Fig. 6c provides a

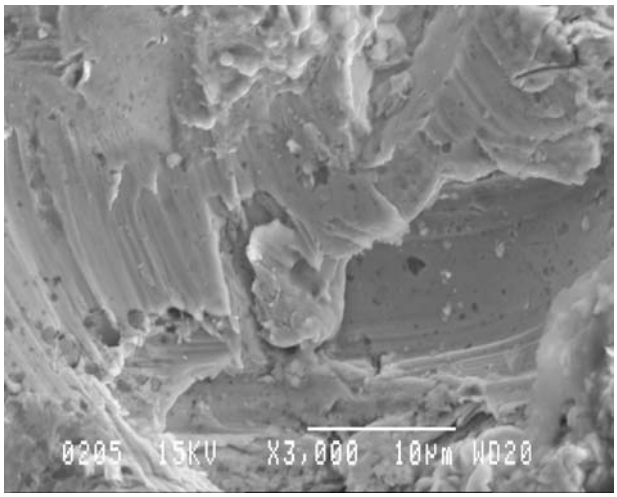

(a)

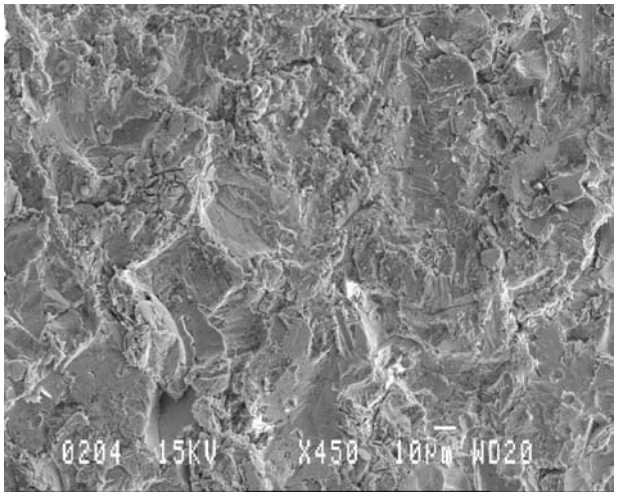

(b)

Figure 5 Scanning electron microscope images of erosion sites: (a) Ploughing tracks, scale bar: 10 μm and (b) Platelet accumulation, scale bar: 10 μm.

close look at a highly strained thin platelet, formed by a mechanism described in [7], that is partly broken. Therefore, the three basic mechanisms assumed for the erosion of ductile materials by angular erodents could be observed during the material removal process. For the conditions in this study, however, platelet formation was the dominant mechanism for material removal, but micro-machining did happen in some situations, probably when the local impact angles differed from 90°.

The distribution of the debris size (S) is shown in Fig. 7. Fig. 7a shows a histogram where the comulative debris number (in percent) is plotted against the debris size. Most of all debris have sizes of about 20 μm which agrees with results in [8]. About 92% of all debris are smaller than the average grain size of the target material. Fig. 7b shows the statistical mean size, and the (graphically estimated) 50%-value. The mean size is about 14 μm which is in the same order of magnitude as values reported in [8] for plain carbon steel, and the 50%-value is $S_{50} = 9.9$ μm. As evidenced in Fig. 7a more that 90% of all debris are smaller than the grain size of the target material. A transgranular erosion mode is, therefore, rather unlikely. The debris are more

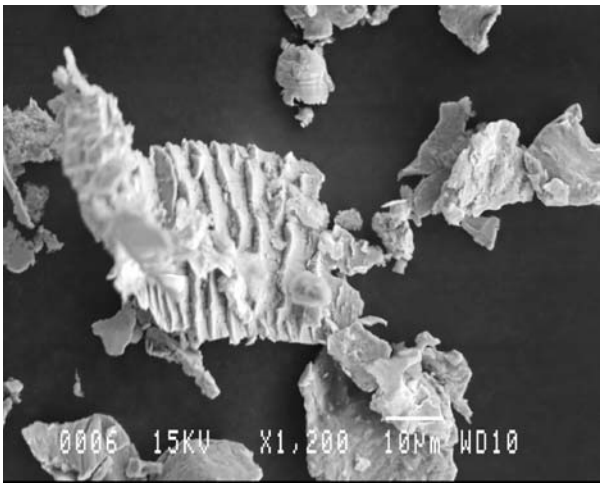

(a)

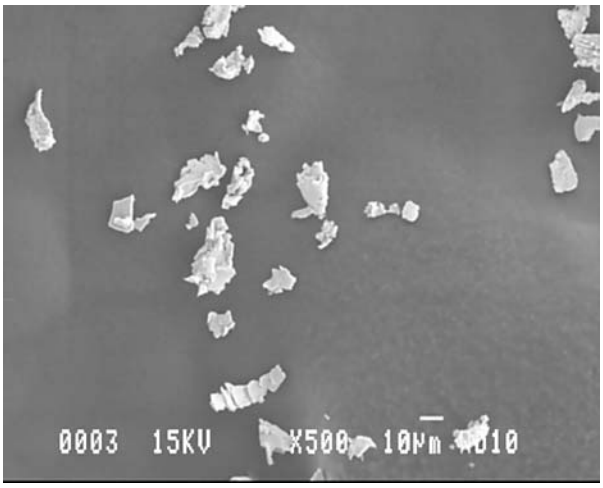

(b)

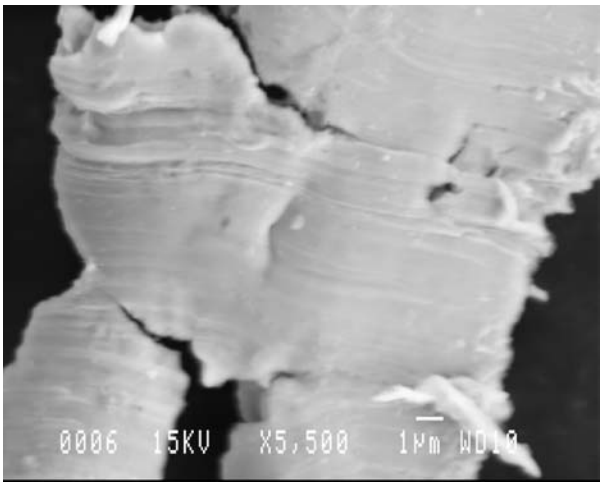

(c)

Figure 6 Scanning electron microscope images of wear debris: (a) Lamellae-type debris (flow-type chip) and platelet type debris, scale bar: 10 μm, (b) Collection of platelets, scale bar: 10 μm, and (c) Highly strained platelet-shaped debris, partly broken, scale bar: 1 μm.

likely only by-products of the crater formation process. Debris are either detached lips from craters formed through ploughing, as evidenced in [5], or platelets detached from the rims of 'smear' craters, as suggested in [7]. It may be considered, however, that debris size as defined by Equation 3 does not allow a distinction

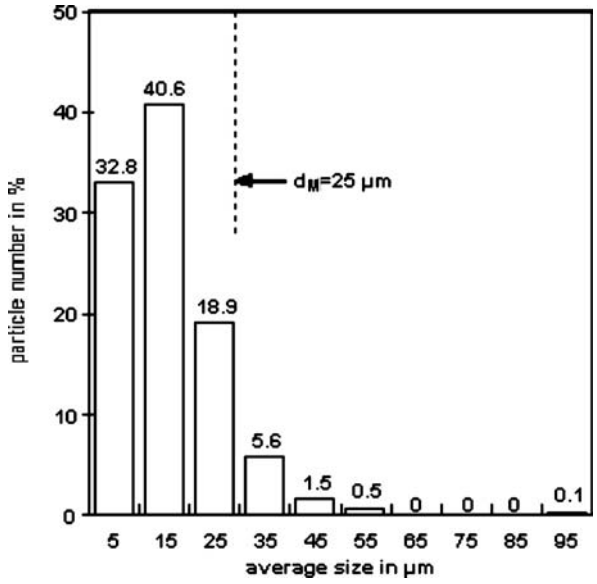

(a)

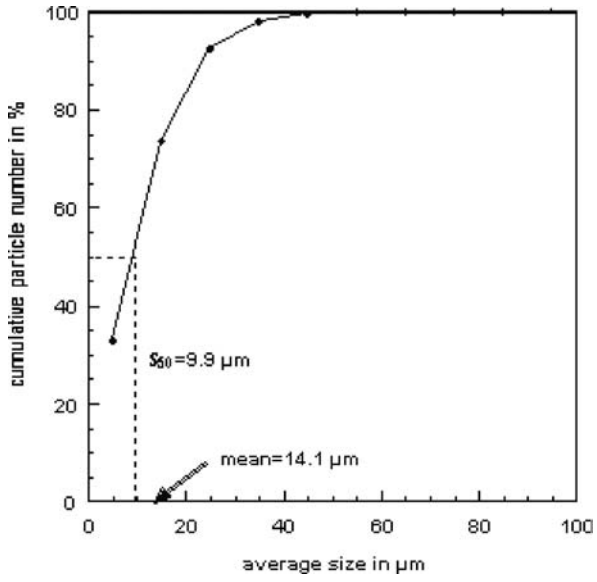

(b)

Figure 7 Size distribution of the analysed wear debris: (a) Histogram and (b) Cumulative distribution.

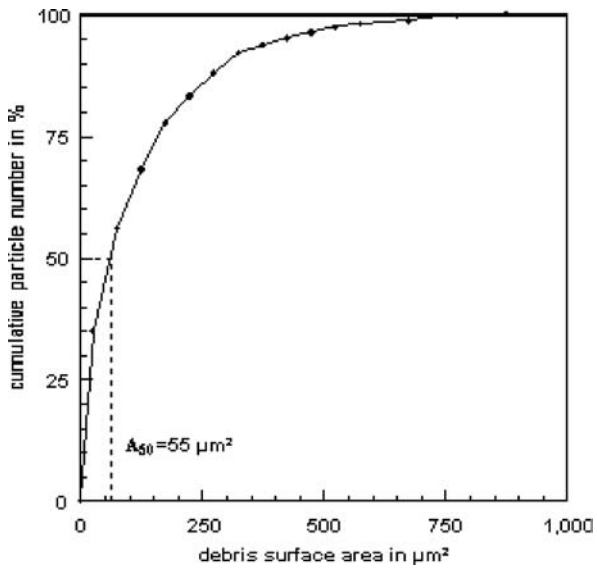

Figure 8 Cumulative area distribution of the analysed wear debris.

between individual shapes, namely between platelets and micro-cutting chips.

The cumulative distribution of the debris surface area is shown in Fig. 8. The statistical mean debris surface area is about 161 μm^2. Although areas as large as 8,000 μm^2 were detected by the image analyser, these large values were most probably the result of adhering platelets as shown in Fig. 6b. They were omitted and not considered for the analysis. Small debris areas were dominating; about 50% of all debris had values less than 70 μm^2. Again, this value is notably smaller than the average cross section of the target material grains (which is 490 μm^2 if a circle with a diameter of 25 μm is assumed).

4. Summary

From the point of view of wear debris geometry, three different types can be distinguished during the erosion of a ductile steel due to the impingement of sharp solid particles. Based on aspect ratio calculations from image analysis results, the most frequent debris type observed was a platelet-type debris as suggested by the Bellman-Levy model. This wear debris shape covered about 60% of all acquired debris. Lip detachment as suggested by Winter and Hutchings also contributed to the erosion. Plain micro-machining according to Finnie's model, however, played a negligible role only. The statistical mean size of the debris was notably smaller that the target grain size. The results supported the figure that 'secondary' removal modes - the detachment of lips or, respectively, platelets from crater rims—were responsible for material removal.

Acknowledgements

The first author thanks the German Research Association (DFG), Bonn, Germany, for financial support. Thanks are also addressed to IRIS, Melbourne, Australia, for technical support.

References

1. A. LEVY, "Solid Particle Erosion and Erosion-Corrosion of Materials" (ASM International, Materials Park, 1995).
2. A. W. MOMBER and R. KOVACEVIC, "Principles of Abrasive Water Jet Machining" (Springer Ltd., London, 1998).
3. P. SHEWMON and G. SUNDARARAJAN, *Ann. Rev. Mater. Sci.* **13** (1983) 301.
4. I. FINNIE, in "Proc. 3rd National Congr. of Applied Mechanics," edited by R. M. Haythornthwaite *et al.* (ASME, New York, 1958) p. 527.
5. R. E. WINTER and I. M. HUTCHINGS, *Wear* **29** (1974) 181.
6. T. H. KOSEL, Z. Y. MAO and S. V. PRASAD, *ASLE Trans.* **28** (1984) 268.
7. R. BELLMANN and A. LEVY, *Wear* **70** (1981) 1.
8. A. HAMMERSTEN, S. SÖDERBERG and S. HOGMARK, in "Proceedings of the International Conference on Wear of Materials," edited. W. A. Glaeser (ASME, New York, 1983) p. 373.
9. S. TSCHERNY, E. WANDTKE and U. FRÖHNER, *Schmierungstechnik* **19** (1988) 235.
10. A. W. MOMBER, H. KWAK and R. KOVACEVIC, *ASME J. Tribol.* **118** (1996) 759.

Received 22 July 2003
and accepted 12 August 2004